

Gross, microscopic, radiologic, echocardiographic and haematological findings in rats experimentally infected with *Angiostrongylus cantonensis*

Research Article

Cite this article: Wun MK, Davies S, Spielman D, Lee R, Hayward D, Malik R (2021). Gross, microscopic, radiologic, echocardiographic and haematological findings in rats experimentally infected with *Angiostrongylus cantonensis*. *Parasitology* **148**, 159–166. <https://doi.org/10.1017/S0031182020001420>

Received: 29 April 2020

Revised: 28 July 2020

Accepted: 29 July 2020

First published online: 3 August 2020



Key words:

Angiostrongylus cantonensis; computed tomography; pathology; radiology; rats; ultrasonography

Author for correspondence:

Matthew K. Wun,

E-mail: mwun8768@uni.sydney.edu.au

Matthew K. Wun¹ , Sarah Davies², Derek Spielman¹, Rogan Lee³, Doug Hayward⁴ and Richard Malik^{5,6} 

¹Sydney School of Veterinary Science, The University of Sydney, Camperdown, NSW 2006, Australia; ²Veterinary Imaging Associates, 52–56 Atchison St, St Leonards, NSW 2065, Australia; ³Centre for Infectious Diseases & Microbiology Laboratory Services, ICPMR, Westmead Hospital, NSW 2145, Australia; ⁴Vetnostics, 60 Waterloo Road, Macquarie Park, NSW 2113, Australia; ⁵Centre for Veterinary Education, The University of Sydney, Camperdown, NSW 2006, Australia and ⁶School of Veterinary and Animal Science, Charles Sturt University, Wagga Wagga, NSW 2678, Australia

Abstract

Although the gross and microscopic pathology in rats infected with *Angiostrongylus cantonensis* has been well described, corresponding changes detected using diagnostic imaging modalities have not been reported. This work describes the cardiopulmonary changes in mature Wistar rats chronically infected with moderate burdens of *A. cantonensis* using radiology, computed tomography (CT), CT angiography, echocardiography, necropsy and histological examinations. Haematology and coagulation studies were also performed. Thoracic radiography, CT and CT angiography showed moderately severe alveolar pulmonary patterns mainly affecting caudal portions of the caudal lung lobes and associated dilatation of the caudal lobar pulmonary arteries. Presumptive worm profiles could be detected using echocardiography, with worms seen in the right ventricular outflow tract or straddling either the pulmonary and/or the tricuspid valves. Extensive, multifocal, coalescing dark areas and multiple pale foci affecting the caudal lung lobes were observed at necropsy. Histologically, these were composed of numerous large, confluent granulomas and fibrotic nodules. Adult worms were found predominantly in the mid- to distal pulmonary arteries. An inflammatory leukogram, hyperproteinaemia and hyperfibrinogenaemia were found in most rats. These findings provide a comparative model for *A. cantonensis* in its accidental hosts, such as humans and dogs. In addition, the pathological and imaging changes are comparable to those seen in dogs infected with *Angiostrongylus vasorum*, suggesting rats infected with *A. cantonensis* could be a model for dogs with *A. vasorum* infection.

Introduction

In its definitive host, the rat, adults of the metastrongylid nematode *Angiostrongylus cantonensis* reside in the pulmonary arteries. Female worms lay eggs, that embolize to the distal pulmonary arteries (Mackerras and Sandars, 1955). Upon hatching from egg nests, first-stage larvae (L_1) penetrate the alveolar walls and induce granulomatous inflammation in the pulmonary interstitium and alveolar spaces, becoming enclosed by loosely-structured granulomas from 45 days post-infection (Hsu *et al.*, 2005; Garcia *et al.*, 2014). By 90 days post-infection, granulomas become fibrotic, leading to alveolar destruction and pulmonary fibrosis (Hsu *et al.*, 2005; Tu and Lai, 2006). These lesions appear grossly as nodules (2–5 mm diameter) in the lung parenchyma (Lee *et al.*, 1996; Tiwari *et al.*, 2018). Adult worms remain in the pulmonary arteries (Garcia *et al.*, 2014) causing intimal hyperplasia and thrombosis due to physical trauma to the vessel walls (Lee *et al.*, 1996; Chikweto *et al.*, 2009) and the increased vascular resistance likely induces pulmonary hypertension. Other gross changes include variable degrees of petechiation and congestion in the lung (Chikweto *et al.*, 2009). The appearance of these pulmonary changes in rats using radiography, computed tomography (CT) or ultrasonography has not been described.

In accidental hosts, such as humans, it is often assumed that lungworm third- and fourth-stage larvae localize in the central nervous system (CNS) until their death, where they cause eosinophilic meningitis and sometimes encephalitis, myeloradiculitis and/or peripheral radiculoneuritis (Lunn *et al.*, 2012; Barratt *et al.*, 2016). However, when organs outside the CNS are examined at necropsy, worms are commonly found within the pulmonary arteries (Prociv, 1999) and evidence of pneumonia and pulmonary haemorrhage have been reported (Yii *et al.*, 1968). Several pulmonary changes have been described in thoracic radiological studies of infected humans (Shih *et al.*, 1992; Cui *et al.*, 2011). CT scans demonstrated variable numbers of nodules (0.5–2.0 cm diameter) in the subpleural region, with some containing round or stick-shaped areas of denser opacity presumed to be worms (Cui *et al.*, 2011). One to four weeks post-infection, ground-glass opacities were evident surrounding nodules

or within the subpleural space. These were thought to be eosinophilic infiltrates, based on the peripheral eosinophilia in these patients. One to two months post-infection, bronchiectasis and pleural thickening, adhesions and indentations were observed, consistent with fibrosis. Ground-glass opacities were not seen at this late stage, correlating with decreased peripheral eosinophilia. This changing appearance is likely due to fibrosis replacing inflammation with resolution. Patchy opacities and air bronchograms in thoracic radiographs of infected humans suggest segmental inflammation in the lower lung fields, and cystic lesions consistent with pulmonary arterial thrombosis have been reported (Shih *et al.*, 1992; Prociw, 1999).

Rats infected with *A. cantonensis* can show regenerative anaemia, thrombocytopenia, neutrophilia, eosinophilia, basophilia and lymphocytosis, variably present from 1 to 8 weeks post-infection (Garcia *et al.*, 2014). Peripheral eosinophilia is the only consistent finding reported in infected humans and dogs (Lunn *et al.*, 2012; Sawanyawisuth *et al.*, 2013). Coagulation studies in rats or accidental hosts with *A. cantonensis* infection have not been performed and haemorrhagic diatheses have not been observed.

This project aims to correlate the gross and microscopic changes in the lungs of rats chronically infected with *A. cantonensis* with findings evident on radiography, CT and non-selective CT angiography and echocardiography. These findings in the definitive host may serve as a comparative model to better understand the pulmonary pathological and imaging changes caused by *A. cantonensis* in its accidental hosts, such as humans and dogs. The lack of radiologic studies in rats and limited histologic studies in humans limits our ability to correlate findings between these two modalities, and a better understanding may allow the pathological changes caused by *A. cantonensis* in the lungs of accidental hosts to be more accurately inferred from imaging findings. In addition, we explored haematologic changes in infected rats and their coagulation status.

Materials and methods

Animal ethics approval was granted from Western Sydney Local Health District/Westmead Animal Ethics Committee (Protocol number: 8003.03.18) to use rats that would otherwise be culled from an *A. cantonensis*-infected colony maintained at the Centre for Infectious Disease & Microbiology Laboratory Service, Westmead Hospital. These rats are used to produce *A. cantonensis* antigen and nucleic acid, used for *A. cantonensis* ELISA testing for humans and dogs, and to support various research projects in Australia and overseas. Rats are culled after 12 months, or sooner if they lose weight or show signs of respiratory distress.

Three Wistar rats with chronic, patent *A. cantonensis* infection (i.e. L_1 in faeces) (rats 1–3) and one Wistar rat with non-patent infection (i.e. no L_1 in faeces) (rat 4) were used for diagnostic imaging, gross pathological and histopathological studies. A further four rats (rats 5–8) with patent infection and three rats (rats 9–11) with non-patent infection were used for haematological and coagulation testing. Although the rats with non-patent infection had been previously infected with *A. cantonensis*, the absence of L_1 in their feces and mature worms in their pulmonary arteries at necropsy indicated the infections had resolved spontaneously. Details of all rats used (weight, infection status, age when first infected and age at the time of our study) are summarized in Table 1.

Diagnostic imaging, gross pathology and histopathology

Following a brief physical examination, rats 1–4 were imaged, then euthanized and necropsied. Procedures were performed in the following order:

- (1) CT. Rats were anaesthetised using ketamine (50 mg) and midazolam (2.5 mg) administered intraperitoneally (rats 1 & 2) or isoflurane (given to effect) in 100% oxygen using a non-rebreathing system and an out-of-circuit vaporizer (rats 3 & 4), and placed in sternal recumbency on the gantry of a GE LightSpeed® 16 Slice CT scanner, with thoracic limbs extended cranially and pelvic limbs extended caudally, both being secured with adhesive tape. CT images were acquired using a 0.625 mm slice thickness with 0.3 mm interval. Images were reconstructed at 0.625 mm isotropic resolution using a medium- to high-frequency convolution kernel.
- (2) Echocardiography and ultrasound of the lung parenchyma. Anaesthesia was maintained with 0.75% isoflurane to facilitate echocardiography and spectral pulsed and continuous wave Doppler studies using a GE Vivid® S5 ultrasound system and 12S-D phased-array cardiac sector transducer using the 12 MHz setting. In rat 1, isoflurane was then increased to 2% to reduce cardiac output, in an attempt to change the location of worms in the pulmonary arteries. Ultrasound of the lung parenchyma was performed using a Philips Affiniti® 70G with an L12–5 linear array transducer using the 12 MHz setting.
- (3) Radiology. Anaesthesia was maintained with isoflurane (1.5%) and left lateral, right lateral, dorsoventral and ventrodorsal radiographs were obtained using a technique chart designed for small mammals.
- (4) Non-selective CT angiography. Anaesthesia was maintained with a second dose of ketamine (50 mg) and midazolam (2.5 mg) intraperitoneally (rat 2) or isoflurane (1.5%) (rat 3), and the rats positioned on the CT scanner gantry as previously described. Iohexol was used as the intravenous contrast agent with an intended dose of 880 mg iodine kg^{-1} . Iohexol (350 mg iodine mL^{-1}) was injected by hand into the lateral tail vein using a 23-gauge butterfly needle (rat 2: 700 mg, rat 3: 525 mg) and the scan commenced a few seconds after the end of injection. Due to technical difficulty finding and injecting into the tail vein and suboptimal vascular opacification in rat 3, a further 700 mg of iohexol was injected and the scan immediately repeated. CT images were acquired using a 0.625 mm slice thickness with 0.3 mm interval. Images were reconstructed at 0.625 mm isotropic resolution using a medium- to high-frequency convolution kernel. Standard viewing software (eFilm Workstation®, MERGE Healthcare, an IBM company, Mississauga, ON, Canada) was used to view CT (and radiographic) images.
- (5) Necropsy. Following euthanasia by an overdose of ketamine and isoflurane (rats 1 & 2) or pentobarbitone sodium (Lethobarb®) (rats 3 & 4), rats were necropsied, and the hearts and lungs removed to be examined grossly. A concerted effort was made to examine the full length of the main pulmonary arteries, as well as the right ventricle and right ventricular outflow tract, to harvest all the lungworms present. Extracted worms were counted and identified as male or female based on morphology.
- (6) Histology. Hearts and lungs were fixed in 20 times their volume of 10% neutral buffered formalin for a minimum of 24 h, then embedded in paraffin, cut to 5 μm thick tissue sections, mounted on glass slides and stained with haematoxylin and eosin (H&E). Sections were examined using conventional light microscopy.

Haematological and coagulation studies

Following brief physical examination and measurement of oxygen saturation (SpO_2) levels with pulse oximetry, rats 5–7 were sedated with an intraperitoneal injection of ketamine (50 mg) and midazolam (2.5 mg) and blood obtained *via* left ventricular

Table 1. Rats used for our investigations, with their weight and infection status determined by the presence (patent infection) or absence (resolved infection) of *L*₁ in their feces

Rats investigated	Weight (g)	Infection status with <i>A. cantonensis</i>	Age when infected	Age at time of investigations	Anaesthetic or method for euthanasia	Worms visualized with echocardiography
Rat 1	600	Patent infection	Unknown	Unknown	Ketamine/Midazolam induction, isoflurane maintenance	No
Rat 2	600	Patent infection	Unknown	Unknown	Ketamine/Midazolam induction, isoflurane maintenance	Yes
Rat 3	530	Patent infection	Unknown	Unknown	Isoflurane	Yes
Rat 4	920	Resolved infection	Unknown	Unknown	Isoflurane	Not attempted
Rat 5	Unknown	Patent infection	Unknown	Unknown	Ketamine/Midazolam	Not attempted
Rat 6	Unknown	Patent infection	Unknown	Unknown	Ketamine/Midazolam	Not attempted
Rat 7	819	Patent infection	6 months	18 months	CO ₂	Not attempted
Rat 8	830	Patent infection	6 months	16 months	CO ₂	Not attempted
Rat 9	745	Resolved infection	6 months	18 months	CO ₂	Not attempted
Rat 10	796	Resolved infection	6 months	17 months	CO ₂	Not attempted
Rat 11	823	Resolved infection	6 months	16 months	CO ₂	Not attempted

puncture. In the remaining rats (rats 8–11), blood was collected *via* left ventricular puncture immediately following euthanasia with 100% CO₂. Samples in EDTA tubes were transported to Veterinary Pathology Diagnostic Services, Sydney School of Veterinary Science, The University of Sydney for haematological analysis (rats 5–11) and citrated plasma samples sent to Vetnostics Laboratory, North Ryde to determine prothrombin time (PTT), activated partial thromboplastin time (aPTT), thrombin time (TT) and fibrinogen and D-dimer levels (rats 6–11).

Results

Diagnostic imaging, gross necropsy findings and histological examination of rats with patent *A. cantonensis* infection (rats 1–3)

Rats were outwardly normal on physical examination, with no discernible tachypnoea or dyspnoea observed. SpO₂ readings obtained were in the range of 93–97%. Radiography showed a moderate to severe alveolar pattern primarily affecting caudal portions of the left and/or right caudal lung lobes (Fig. 1A and E). Pulmonary vessels were difficult to assess in the radiographic studies due to the small size of the thorax and increased pulmonary parenchymal opacity causing border effacement of the vessels. Air bronchograms could be seen in the most severely affected portions of the lung. Changes in pulmonary opacity were typically asymmetrical. These observations were confirmed by the CT studies, which also showed enlargement of the caudal lobar pulmonary arteries (Fig. 1B, C, F and G). These changes were more obvious in CT angiography images. Negative worm profiles could not be discerned within the pulmonary arteries. Subjectively, the heart was normal in size and shape, and dilatation of the main pulmonary artery segment was not appreciated radiologically. In the most severely radiographically affected rat (rat 2), areas of increased pulmonary opacity were identified in the accessory, right cranial and middle lung lobes on CT, in addition to the caudal lobar regions.

Echocardiographic observations varied between rats. There was no detectable cardiac chamber enlargement and the main pulmonary artery was of normal size and appearance. It was sometimes possible to interrogate hyperechoic parallel structures (up to 10 mm in length in some views) resembling worm profiles

in transverse and short longitudinal section (Fig. 2). In other rats, this was not possible despite concerted efforts, presumably because worms were in portions of the pulmonary arterial tree beyond the acoustic window of the ultrasound beam. Presumptive worm profiles, when encountered, were detected in the right ventricular outflow tract just below the level of the pulmonary valve or straddling either the pulmonary or the tricuspid valves. Attempts to change the location and number of worm profiles by varying the inspired concentration of isoflurane (and hence anaesthetic depth and cardiac output) failed. Pulmonary hypertension was suggested in one rat using spectral Doppler echocardiography to detect a high velocity (3–4 m s⁻¹) regurgitant jet through the pulmonary artery. Ultrasound of the caudal lung lobe parenchyma showed hepatisation with complex heterogeneous echogenicity and comet tail artefacts (Fig. 1J).

Pulmonary lesion distribution was confirmed by necropsy examination, with extensive, multifocal coalescing areas of dark discolouration (consolidation) and multiple pale foci (<1 mm diameter) affecting one or both caudal lung lobes (Fig. 1D and H). The cranial lung lobes were variably but generally much less severely affected. The demarcation between abnormal and normal lung was often sharply delineated. Distal pulmonary arteries were dilated, sometimes segmentally, with a focal portion harbouring a knot of tangled coiled lungworms. Adult male and female lungworms were located predominantly in the mid to distal pulmonary arteries (Fig. 1I), although in rat 2 a single worm was also found in the right ventricular outflow tract just below the pulmonary valve. All worms were non-motile and presumably dead upon removal. The number and sex of the lungworms in the investigated rats were as follows: rat 1 had 9 worms (4 males, 5 females), rat 2 had 10 worms (3 males, 7 females) and rat 3 harboured 12 worms (5 males, 7 females). Male worms were thin and did not display the 'barber's pole' appearance; female worms were longer and thicker and had a barber's-pole appearance due to the gut containing blood and digested blood wrapping around the ovaries (Mackerras and Sandars, 1955). The heart in all rats appeared grossly normal.

Histologic examination of the caudal lung lobes showed replacement of normal tissue architecture with numerous small to large confluent granulomas and fibrotic nodules (Fig. 1K). Granulomas consisted of oval spaces containing parasitic eggs

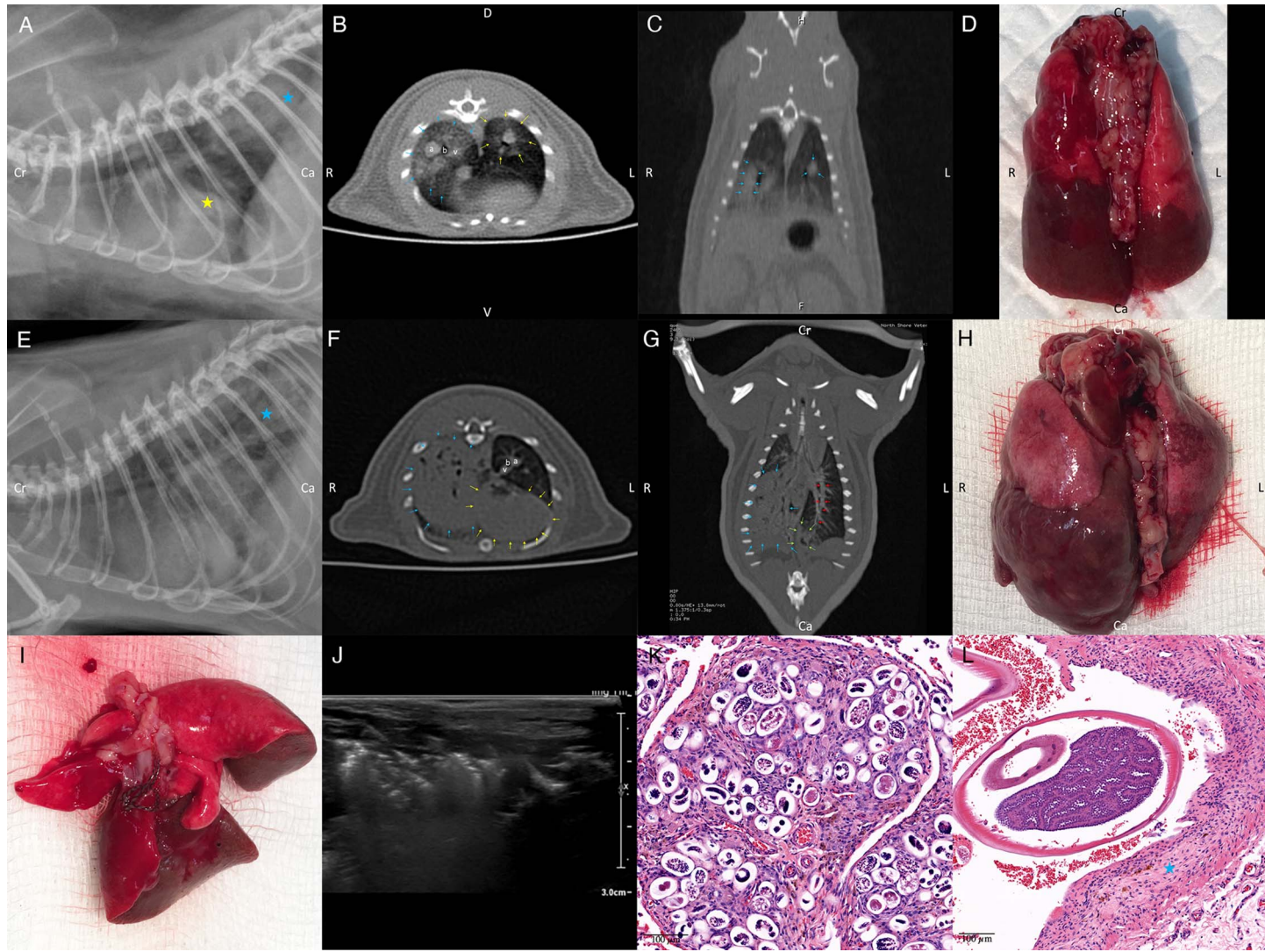


Fig. 1. (A) Left lateral radiograph of rat 3. An alveolar pattern is present in the caudal lobar region (blue star) and a poorly demarcated increase in soft tissue opacity is superimposed over the caudal margin of the cardiac silhouette (yellow star). Cardiac margins are poorly demarcated. (B) Axial CT angiography image of rat 3 at the level of the cardiac apex. The left and right caudal lobar pulmonary arteries are markedly enlarged. A ground glass soft tissue opacity is present in the right caudal lung lobe (blue arrows) and to a lesser degree in the left caudal lung lobe (yellow arrows). Right caudal pulmonary artery (a) together with bronchus (b) and pulmonary vein (v). (C) Dorsal reconstructed CT image of rat 3 through the caudal lung lobes. Caudal pulmonary lobar arteries are enlarged and do not taper normally (blue arrows). A ground glass soft tissue opacity is present in the right and to a lesser degree left caudal lung lobes. (D) Dorsal aspect of the lungs of rat 3 at necropsy. Note extensive, multifocal coalescing areas of dark discolouration (consolidation) of the caudal aspects of the lung lobes, worse on the right. N.B. this image has been flipped horizontally to correspond with the CT images. (E) Left lateral radiograph of rat 2. A marked multifocal alveolar pattern is present in the caudal lobar region (blue star). Cardiac margins are poorly demarcated. Axial (F) and dorsal reconstructed (G) CT images of rat 2 made through the caudal lung lobes. The right caudal lung lobe (blue arrows) appears consolidated with small remaining gas opacities associated with bronchial structures. A more focal region of alveolar disease is present in the caudal and medial extremity of the left caudal lung lobe (green arrows), at the terminal aspect of the lobar artery (red arrows). An alveolar pattern is also present in the accessory lung lobe, immediately dorsal to the heart (yellow arrows). Enlarged left caudal pulmonary artery (a), together with bronchus (b) and pulmonary vein (v). (H) Dorsal aspect of the lungs of rat 2 at necropsy. Note the extensive, multifocal coalescing areas of dark discolouration (consolidation) of the right caudal lung lobe and caudal aspect of the left lung lobe, more marked on the right. N.B. this image has been flipped horizontally to better correspond to the CT images. (I) Dissected lungs of rat 3 *ex vivo*, ventral surface. Numerous mature lungworms can be seen in the left distal pulmonary arteries. (J) Ultrasound appearance of partially hepatized caudal lung lobe regions from rat 3. Note the complex heterogeneous echogenicity and comet-tail artifact due to residual gas within the markedly abnormal lung parenchyma. (K and L) Histological images of lungs from rat 3, stained with H&E. (K) A granuloma consisting of parasitic eggs and first-stage larvae surrounded by many plump fibroblasts and collagen, numerous large macrophages plus lymphocytes, plasma cells, scattered neutrophils and occasional eosinophils can be seen. (L) Transverse sections of adult worms can be seen within a pulmonary artery. Note the thickened vascular walls (blue star).

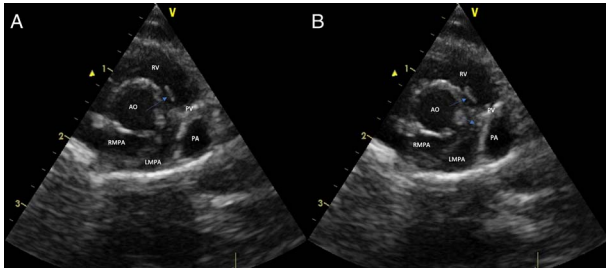


Fig. 2. Right parasternal short axis echocardiographic view of the heart at the level of the heart base and pulmonary artery of a rat (rat 2) chronically infected by *A. cantonensis*. The blue arrows denote worm profiles in the right ventricular outflow tract and straddling the pulmonary valve. (A and B) represent two different frames separated slightly in time. RV, right ventricle; AO, aorta; PV, pulmonary valve; PA, pulmonary artery; LMPA, left main pulmonary artery; RMPA, right main pulmonary artery.

and L_1 surrounded by many plump fibroblasts and collagen, numerous large macrophages plus lymphocytes, plasma cells, scattered neutrophils and occasional eosinophils. Many of these granulomas contained abundant dilated capillaries and small to large haemorrhages, while others were calcified. Fibrotic nodules consisted of swirls of dense fibrous tissue with only scattered oval spaces containing L_1 with occasional eggs. The most well-vascularized fibrous tissue was infiltrated by numerous plasma cells and many plump macrophages including multi-nucleated giant cells, lymphocytes and scattered eosinophils. Some sections were composed predominantly of granulomas (rats 1 & 3), while others had mainly fibrotic nodules (rat 2). Normal but congested alveoli were variably present. In areas with no remaining alveoli, some remnant airways contained numerous L_1 . Transverse sections of adult worms were also observed in the pulmonary arteries in some sections (Fig. 1L). Worms were seen in vessels with thickened walls without red blood cells (possibly lymphatics) and pulmonary arteries with walls thickened by fibrous tissue and infiltrating macrophages, lymphocytes, plasma cells and eosinophils, with groups of erythrocytes between the worm cross-sections (Fig. 1L). Worms within pulmonary arteries were occasionally associated with thrombi. The myocardium was normal histologically.

Diagnostic imaging, gross pathology and histopathology of a rat with resolved *A. cantonensis* infection (rat 4)

Aside from appearing overweight, physical examination was unremarkable with no tachypnoea or dyspnoea observed. Radiographs appeared normal but CT studies demonstrated slightly increased opacity in the caudodorsal portions of the caudal lung lobes. Caudal lobar pulmonary arteries and veins appeared subjectively enlarged on CT. Grossly, the caudal portion of the caudal left lung lobe had a focal area of dark discolouration and multiple foci of pale discolouration (<1 mm diameter) were found on the remaining surface of the left lung lobe. The right lung lobes appeared normal. Pulmonary arteries appeared normal and contained no adult worms. Histologically, most of the pulmonary interstitium was infiltrated by numerous macrophages, lymphocytes and plasma cells accompanied by fibrosis (interstitial pneumonia). Less affected areas showed a loss of alveolar spaces due to alveolar collapse. There was moderate congestion and haemorrhage with multiple deposits of haemosiderin and haemosiderophages and several thrombi within the pulmonary vasculature. No worms or eggs were observed.

Haematology in rats with patent (rats 5–8) and resolved (rats 9–11) *A. cantonensis* infection

Haematological results are summarized in Tables S1 and S2, with published normal reference intervals for male Wistar rats. The

haematological findings were variable, and the small sample size precluded statistical analysis.

Rats with patent infection showed mild hyperproteinaemia (rats 5–8), mild erythrocytosis (rat 5), mildly decreased MCV (rats 5 & 6), mildly decreased MCHC (rats 7 & 8), mildly decreased MCH (rats 5 & 6), moderate leucocytosis (rat 8) with a mild neutrophilia (rats 6 & 8), moderate monocytosis (rats 5–8), moderate eosinophilia (rat 8) and mild basophilia (rat 8).

Rats with resolved infection showed moderate hyperproteinaemia (rats 9–11), mildly reduced haemoglobin concentration (rat 11), mildly decreased MCHC (rats 9–11), mildly decreased MCH (rat 9), mild-moderate leucocytosis (rats 9–11) with a mild neutrophilia (rat 9), moderate monocytosis (rats 9–11), mild-moderate eosinophilia (rats 9–11) and mild basophilia (rats 9–11).

Coagulation studies in rats with patent (rats 6–8) and resolved (rats 9–11) *A. cantonensis* infection

Results from coagulation studies are summarized in Tables S3 and S4, with published reference intervals of male Wistar rats. Rats with patent infection showed mildly decreased PTT (rats 6–8), mild hyperfibrinogenaemia (rats 7 & 8) and moderately-markedly prolonged TT (rats 6–8). aPTT and D-dimer levels were within reference intervals. Rats with resolved infection showed mildly decreased PTT (rats 9–11), mild-moderate hyperfibrinogenaemia (rats 10–11) and moderately-markedly prolonged TT (rats 6–8). aPTT and D-dimer levels were within reference intervals.

Discussion

Although the gross and microscopic lesions of naturally occurring and experimental *A. cantonensis* infection in rats have been documented, there are no reports concerning the radiographic, CT or CT angiography findings. Furthermore, it was not known if it is possible to visualize these parasitic nematodes *in vivo* using two-dimensional echocardiography. Relatively consistent radiological findings were observed in Wistar rats with experimental infections, although the findings varied from rat to rat, likely attributable to the worm burden and the anatomical location of the worms. Echocardiography in two out of three individuals demonstrated worm profiles in the right ventricular outflow tract and main pulmonary artery, but the ultrasound beam was unable to interrogate the more distal pulmonary arteries where worms are typically situated.

Radiographs and CT demonstrated multifocal moderate to severe alveolar disease, primarily affecting the caudal lung lobes, mostly involving their caudal extremities. Changes were typically asymmetrical and more severe on the right. Radiographic and CT findings were supported by gross and microscopic examinations of the lungs post-mortem, which demonstrated that the extensive, multifocal coalescing areas of discolouration with multiple pale foci were composed of numerous small to large confluent egg granulomas and fibrotic nodules. The pathologic changes in the lung are consistent with those reported in the literature (Lee *et al.*, 1996; Hsu *et al.*, 2005; Tu and Lai, 2006; Garcia *et al.*, 2014; Tiwari *et al.*, 2018) and likely reflect the embolization of eggs to distal pulmonary arterioles, where L_1 subsequently hatch to penetrate the alveoli of the subserved lung parenchyma, inducing a florid inflammatory response which then becomes fibrotic. Sections of adult worms seen during histological examination of infected lungs indicate that not all worms were removed during our dissection; a technique such as macerating the lung to small pieces would be required to do this adequately.

In humans, a similar lesion distribution is observed radiographically (Shih *et al.*, 1992) and granulomas can be visualized

on CT as subpleural nodules surrounded by areas of ground-glass opacity merging with areas of consolidated lung (Cui *et al.*, 2011). Although we observed similar granulomas grossly and microscopically, the small size of rats might have compromised our ability to visualize these changes on CT. Also, we used a human 16 slice scanner rather than a microCT specifically designed for rodents (Clark and Badea, 2014).

In rats with lungworm disease, the caudal lobar pulmonary arteries were enlarged on CT images. This was considered a consequence of worm burden in the lumen of the pulmonary arteries, plus the associated thrombosis, causing dilatation proximally. Microscopically, there was concurrent thickening of the pulmonary arterial walls attributable to trauma from the movements of the worms, as reported (Lee *et al.*, 1996; Chikweto *et al.*, 2009; Garcia *et al.*, 2014). Segmental pulmonary arterial dilatation was confirmed at necropsy, with the dilated segments containing knots of tangled, coiled worms. Pulmonary arterial enlargement, wall thickening and segmental dilatation have not been reported in humans, which may reflect lower relative worm burdens in the pulmonary arteries of accidental hosts, compared to the definitive host.

During the echocardiographic examinations, portions of worm profiles could sometimes be visualized in the right ventricular outflow tract just below the pulmonary valve or straddling either the pulmonary or tricuspid valves. Transverse profiles were likely multiple cross-sections of a single coiled worm. This differs from the typical location of worms observed following euthanasia at necropsy, with only one worm found in the right ventricle of a single rat. Remaining worms were found in the distal caudal lobar pulmonary arteries. Under normal physiological conditions, worms likely stay within the pulmonary arteries due to outward blood flow (away from the heart), or to avoid hostile intracardiac haemodynamics and the detrimental effects one or more worms straddling the pulmonary valve would have on the host (Paul Prociw, personal communication). It is possible that reduced cardiac output due to prolonged isoflurane anaesthesia caused worms in some rats to 'fall back' from the pulmonary arteries towards the right ventricle, allowing them to be visualized using echocardiography. However, anaesthetising rats with midazolam/ketamine, a combination thought to better maintain normal cardiac output than isoflurane, followed by varying the inspired concentration of isoflurane, did not reveal more worms. Alternatively, pentobarbitone or midazolam/ketamine used to euthanise the rats might have paralysed or killed the worms, causing them to embolize to the distal branches of the pulmonary arteries. In rats euthanized with CO₂, adult *A. cantonensis* worms remain viable and can be found in the right ventricle, at the pulmonary valve, and within the proximal or distal pulmonary arteries (Chris Niebuhr, personal communication). Further research to experimentally determine the physiological location of the worms is warranted. As worms could not be visualized in every infected rat investigated, we would not recommend this technique as a definitive diagnostic test for wild or pet rats suspected of having *A. cantonensis* infection.

Pulmonary hypertension is likely to develop due to increased pulmonary vascular resistance attributable to adult worms, their eggs and thrombi in pulmonary arteries and arterioles. No evidence of overt heart chamber enlargement or congestive heart failure was observed from radiography, echocardiography or gross examination at necropsy, and no free fluid was observed in either the thoracic or abdominal cavities.

Considering the extensive lesion distribution throughout the lung parenchyma and loss of normal tissue architecture, it is perhaps surprising that infected rats did not exhibit clinical signs of respiratory compromise such as tachypnoea, dyspnoea, cyanosis or other evidence of impaired blood haemoglobin oxygen

saturation due to ventilation-perfusion mismatch. Possible explanations for sufficient oxygenation in the face of the severe pulmonary disease include the low oxygen demand of a sedentary lifestyle and a large respiratory reserve which could be due to selection pressure from the high prevalence of polymicrobial respiratory infections in wild rats (Rothenburger *et al.*, 2015). Further studies measuring oxygen saturation in infected rats during various levels of treadmill activity would be required to better characterize cardiorespiratory dysfunction.

Haematological changes observed were generally mild, with the inflammatory leukogram found in many rats likely reflecting a systemic inflammatory response to the extensive granulomatous inflammation affecting a large portion of the lung parenchyma, with metazoan organisms releasing many antigenic excretory products. Hyperproteinemia and specifically hyperfibrinogenemia seen in all rats tested probably reflected chronic inflammation, as fibrinogen is an acute phase reactant in the rat. Monocytosis could be due to increased demand for macromolecular phagocytosis of eggs and L₁ in the pulmonary alveoli. These changes accord with those reported by Garcia *et al.*, 2014, although we did not observe the regenerative anaemia or thrombocytopenia seen in rats from 3–8 and 6–8 weeks post-infection, respectively. These differences could reflect the chronicity of infection in our rats (10–12 months post-infection). Haematological changes did not differ significantly between rats with patent and resolved infections, which might be due to on-going pneumonia in the later despite the loss of intact adult worms, eggs and larvae. This is supported by histopathological findings suggestive of interstitial pneumonia in the rat with resolved infection (rat 4). Interestingly, the peripheral eosinophilia commonly reported in accidental hosts of *A. cantonensis* (Lunn *et al.*, 2012; Sawanyawisuth *et al.*, 2013) does not appear to be a consistent finding in the definitive host. Hyperfibrinogenemia in most of our rats likely reflects systemic inflammation, with prolonged TT secondary to this, possibly due to binding of thrombin to fibrin or interference with fibrin monomer polymerization by excess fibrinogen (Carr and Gabriel, 1986).

Limitations of our studies include the potential for anaesthesia-induced artefacts in our radiologic findings. In addition, the validity of comparing and consolidating findings between rats might have been impaired by the differing anaesthetic protocols. CT images from rats 1 to 2 were of substantially better quality than those from rats 3 to 4, presumably due to reduced motion artefact from the slower respiratory excursions in rats anaesthetised by midazolam/ketamine (compared to isoflurane).

Despite these limitations, this work provides a comprehensive description of the pulmonary pathology caused by *A. cantonensis* in its definitive host, using a variety of non-invasive and invasive diagnostic techniques. Our findings are reminiscent of the pulmonary dysfunction seen in dogs with *Angiostrongylus vasorum* infections. *A. vasorum* in dogs has a similar lifecycle to *A. cantonensis* in rats, although *A. vasorum* larvae and young adult worms generally remain in the heart and vasculature rather than traversing the CNS (Koch and Willesen, 2009). Infected lung tissue from dogs contain multifocal, coalescing, firm, irregularly discoloured nodules (1–3 mm diameter) on the surface of all lung lobes (Prestwood *et al.*, 1981; Schnyder *et al.*, 2010). These granulomas consist of viable or necrotic larvae and eggs surrounded by macrophages, multi-nucleated giant cells and lymphocytes (Prestwood *et al.*, 1981; Schnyder *et al.*, 2010). Adjacent lung parenchyma exhibits thickened alveolar walls due to an inflammatory infiltrate and pneumocyte hyperplasia, and erythrocytes, haemosiderophages, eosinophils and plasma cells are seen within alveolar spaces (Prestwood *et al.*, 1981; Schnyder *et al.*, 2010). These changes are evident grossly as regions of consolidation and can

involve much of the lung (Prestwood *et al.*, 1981; Schnyder *et al.*, 2010) and manifest radiologically as a multifocal, peripheral, alveolar pattern with air bronchograms (Mahaffey *et al.*, 1981; Boag *et al.*, 2004; Chapman *et al.*, 2004; Kranjc *et al.*, 2010). On CT, large nodules merge with consolidated areas of the lung containing air bronchograms; such lesions occur in all lung lobes surrounded by rims of ground-glass opacity (Koch and Willeesen, 2009; Dennler *et al.*, 2011).

Pathological changes and radiological findings reported in dogs with *A. vasorum* that were not observed in our study of *A. cantonensis* in rats include bronchial wall thickening, pleural fissure lines, pleural effusion, fibrous thickening of the pleura, pleural adhesions and pulmonary lymphadenomegaly (Mahaffey *et al.*, 1981; Prestwood *et al.*, 1981; Boag *et al.*, 2004; Chapman *et al.*, 2004; Kranjc *et al.*, 2010; Schnyder *et al.*, 2010; Dennler *et al.*, 2011), likely reflecting pathophysiological differences between the two parasites. Similar to rats infected with *A. cantonensis*, pulmonary arteries in dogs with *A. vasorum* can have thickened walls and contain thromboses, often containing larvae and eggs (Prestwood *et al.*, 1981; Schnyder *et al.*, 2010). In dogs, enlarged pulmonary arteries are evident on radiographs, and luminal filling defects representing thrombi and/or larvae can be observed with non-selective CT-angiography (Dennler *et al.*, 2011). In our investigations, the limited resolving power of the human imaging equipment used may have made such changes indiscernible.

In dogs, mature *A. vasorum* worms are not detectable in the heart or pulmonary arteries using echocardiography (Nicolle *et al.*, 2006; Kranjc *et al.*, 2010), presumably because worms coil in the terminal pulmonary arterial branches which are not accessible for ultrasound evaluation. Reported changes on echocardiography include pulmonary hypertension, right atrial and ventricular dilation, dilated pulmonary trunk, tricuspid and pulmonary valve insufficiencies and changes in pulmonary flow profiles using a spectral Doppler (Nicolle *et al.*, 2006; Kranjc *et al.*, 2010; Helm and Morgan, 2017). It is interesting that such changes indicative of right-sided heart failure were not observed in our infected rats.

In contrast to *A. cantonensis* in rats, dogs infected with *A. vasorum* can show thrombocytopenia, prolonged PTT, aPTT and one-stage prothrombin time (OSPT), reduced factor V and VIII activity, and elevated D-dimer concentration (Cury *et al.*, 2002; Chapman *et al.*, 2004; Koch and Willeesen, 2009; Schnyder *et al.*, 2010; Adamantos *et al.*, 2015). These changes suggest low-grade disseminated intravascular coagulation (DIC) resulting in a consumptive coagulopathy (Stokol, 2003; Wiinberg *et al.*, 2010; Adamantos *et al.*, 2015). Fibrinogen can be increased or decreased, presumably due to systemic inflammation, or DIC, respectively (Adamantos *et al.*, 2015). DIC may cause the bleeding diatheses seen in 60% of infected dogs (Ramsey *et al.*, 1996; Adamantos *et al.*, 2015). Alternatively, a primary coagulation defect could be responsible, as PTT and aPTT can be normal with haemorrhage (Adamantos *et al.*, 2015). It is possible that the lack of evidence for DIC or a consumptive coagulopathy in our studies could reflect pathophysiological differences between *A. cantonensis* in rats and *A. vasorum* in dogs, although further sampling from rats infected with larger burdens of *A. cantonensis* would be informative.

Concluding remarks

Firstly, characteristic radiological findings of *A. cantonensis* infections in rats allows the disease in its definitive host to be studied non-invasively. Further, it provides a comparative model for lung disease in its accidental hosts, such as humans and dogs. Secondly, visualization of worms with echocardiography could

allow the physiological location of the worms *in situ* to be studied further. Thirdly, because there is a great deal of interest in disease due to *A. vasorum* in dogs in Europe and the UK, rats infected with *A. cantonensis* appear to be a potential laboratory model with similar (but not identical) clinical, radiological and haematological findings. This suggests similar pathophysiological mechanisms for these closely related metastrongylid parasites and might allow the extrapolation of some findings from rats to dogs. Finally, although the diagnosis of patent *A. cantonensis* infection in a pet rat is most easily obtained by examination of feces for *L*₁ (using Baermann apparatus), thoracic radiographs, CT and echocardiography all have a potential role in the assessment of the severity of the infection, which may impact the therapeutic approach to case management.

Supplementary material. The supplementary material for this article can be found at <https://doi.org/10.1017/S0031182020001420>

Acknowledgements. The authors would like to thank Christine Black (Veterinary Pathology Diagnostic Services) and George Reppas (Vetnostics) for their assistance with this project.

Financial support. This work was completed in partial fulfilment for the requirements of the Doctor of Veterinary Medicine degree, The University of Sydney (MKW), and was (in part) funded by the Sydney School of Veterinary Science Research & Enquiry Unit of Study 2018 fund. RM is supported by the Valentine Charlton Bequest of the Centre for Veterinary Education.

Conflict of interest. None.

Ethical standards. The authors assert that all procedures contributing to this work comply with the ethical standards of the relevant national and institutional guides on the care and use of laboratory animals.

References

- Adamantos S, Waters S and Boag A (2015) Coagulation status in dogs with naturally occurring *Angiostrongylus vasorum* infection. *Journal of Small Animal Practice* **56**, 485–490.
- Barratt J, Chan D, Sandaradura I, Malik R, Spielman D, Lee R, Marriott D, Harkness J, Ellis J and Stark D (2016) *Angiostrongylus cantonensis*: a review of its distribution, molecular biology and clinical significance as a human pathogen. *Parasitology* **143**, 1087–1118.
- Boag AK, Lamb CR, Chapman PS and Boswood A (2004) Radiographic findings in 16 dogs infected with *Angiostrongylus vasorum*. *Veterinary Record* **154**, 426–430.
- Carr JME and Gabriel DA (1986) Hyperfibrinogenemia as a cause of prolonged thrombin clotting time. *Southern Medical Journal* **79**, 563–570.
- Chapman PS, Boag AK, Guitian J and Boswood A (2004) *Angiostrongylus vasorum* infection in 23 dogs (1999–2002). *Journal of Small Animal Practice* **45**, 435–440.
- Chikweto A, Bhaiyat MI, Macpherson CNL, Deallie C, Pinckney RD, Richards C and Sharma RN (2009) Existence of *Angiostrongylus cantonensis* in rats (*Rattus norvegicus*) in Grenada, West Indies. *Veterinary Parasitology* **162**, 160–162.
- Clark DP and Badea CT (2014) Micro-CT of rodents: state-of-the-art and future perspectives. *Physica Medica* **30**, 619–634.
- Cui Y, Shen M and Meng S (2011) Lung CT findings of angiostrongyliasis *cantonensis* caused by *Angiostrongylus cantonensis*. *Clinical Imaging* **35**, 180–183.
- Cury MC, Lima WS, Guimarães MP and Carvalho MG (2002) Hematological and coagulation profiles in dogs experimentally infected with *Angiostrongylus vasorum* (Baillet, 1866). *Veterinary Parasitology* **104**, 139–149.
- Dennler M, Makara M, Kranjc A, Schnyder M, Ossent P, Deplazes P, Ohlerth S and Glaus TM (2011) Thoracic computed tomography findings in dogs experimentally infected with *Angiostrongylus vasorum*. *Veterinary Radiology and Ultrasound* **52**, 289–294.
- Garcia JS, Dos Santos Bonfim TC, Junior AM, Tunholi VM, Tunholi-Alves VM, Mota EM, Simões RDO, Santana AC, Hooper C, Pinheiro J and Bóia MN (2014) Hematological and histopathological changes in *Rattus*

- norvegicus* (Wistar) experimentally infected by *Angiostrongylus cantonensis* (Chen, 1935). *Parasitology International* **63**, 631–637.
- Helm J and Morgan E** (2017) Canine and feline lungworm infections in the UK. *In Practice* **39**, 298–315.
- Hsu LS, Lee HH, Chen KM, Chou HL and Lai SC** (2005) Matrix metalloproteinase-2 and -9 in the granulomatous fibrosis of rats infected with *Angiostrongylus cantonensis*. *Annals of Tropical Medicine & Parasitology* **99**, 61–70.
- Koch J and Willesen JL** (2009) Canine pulmonary angiostrongylosis: an update. *The Veterinary Journal* **179**, 348–359.
- Kranjc A, Schnyder M, Dennler M, Fahrion A, Makara M, Ossent P, Morgan J, Deplazes P and Glaus TM** (2010) Pulmonary artery thrombosis in experimental *Angiostrongylus vasorum* infection does not result in pulmonary hypertension and echocardiographic right ventricular changes. *Journal of Veterinary Internal Medicine* **24**, 855–862.
- Lee H-H, Jiang S-T, Shyu L-Y, Lin W-L, Chian H-C, Hsu C-C, Chou F-P and Wang C-J** (1996) L ferritin accumulation in macrophages infiltrating the lung during rat *Angiostrongylus cantonensis* infection. *Experimental Parasitology* **61**, 55–61.
- Lunn JA, Lee R, Smaller J, Mackay BM, King T, Hunt GB, Martin P, Krockenberger MB, Spielman D and Malik R** (2012) Twenty two cases of canine neural angiostrongylosis in eastern Australia (2002–2005) and a review of the literature. *Parasites and Vectors* **5**, 70.
- Mackerras MJ and Sandars DF** (1955) The life history of the rat lung-worm, *Angiostrongylus cantonensis* (Chen) (Nematoda: Metastrongylidae). *Australian Journal of Zoology* **3**, 1–21.
- Mahaffey MB, Losonsky JM, Prestwood AK, Mahaffey EA and Lewis RE** (1981) Experimental canine angiostrongylosis. II. Radiographic manifestations. *The Journal of the American Animal Hospital Association* **17**, 499–502.
- Nicolle AP, Chetboul V, Tessier-Vetzel D, Sampedrano CC, Aletti E and Pouchelon JL** (2006) Severe pulmonary arterial hypertension due to *Angiostrongylus vasorum* in a dog. *Canadian Veterinary Journal* **47**, 792–795.
- Prestwood AK, Greene CE, Mahaffey EA and Burgess DE** (1981) Experimental canine angiostrongylosis. I. Pathologic manifestations. *The Journal of the American Animal Hospital Association* **17**, 491–497.
- Procv P** (1999) Parasitic meningitis. *Medical Journal of Australia* **170**, 517–518.
- Ramsey IK, Littlewood JD, Dunn JK and Herrtage ME** (1996) Role of chronic disseminated intravascular coagulation in a case of canine angiostrongylosis. *Veterinary Record* **138**, 360–363.
- Rothenburger JL, Himsworth CG, Clifford CB, Ellis J, Treuting PM and Leighton FA** (2015) Respiratory pathology and pathogens in wild urban rats (*Rattus norvegicus* and *Rattus rattus*). *Veterinary Pathology* **52**, 1210–1219.
- Sawanyawisuth K, Chindapasirt J, Senthong V, Limpawattana P, Auvichayapat N, Tassniyom S, Chotmongkol V, Maleewong W and Intapan PM** (2013) Clinical manifestations of eosinophilic meningitis due to infection with *Angiostrongylus cantonensis* in children. *Korean Journal of Parasitology* **51**, 735–738.
- Schnyder M, Fahrion A, Riond B, Ossent P, Webster P, Kranjc A, Glaus T and Deplazes P** (2010) Clinical, laboratory and pathological findings in dogs experimentally infected with *Angiostrongylus vasorum*. *Parasitology Research* **107**, 1471–1480.
- Shih SL, Hsu CH, Huang FY, Shen EY and Lin JC** (1992) *Angiostrongylus cantonensis* infection in infants and young children. *The Pediatric Infectious Disease Journal* **11**, 1064–1066.
- Stokol T** (2003) Plasma D-dimer for the diagnosis of thromboembolic disorders in dogs. *Veterinary Clinics of North America – Small Animal Practice* **33**, 1419–1435.
- Tiwari K, Montanez Acuna A, Guerrero A, Piechowski B, Thille K and Sharma RN** (2018) Seroprevalence and pathology of lung worm *Angiostrongylus cantonensis* in brown rats (*Rattus norvegicus*) from Grenada, West Indies. *Indian Journal of Veterinary Pathology* **42**, 32–35.
- Tu WC and Lai SC** (2006) Induction of tumour necrosis factor, interleukin-1b and matrix metalloproteinases in pulmonary fibrosis of rats infected with *Angiostrongylus cantonensis*. *Journal of Helminthology* **80**, 305–311.
- Wiinberg B, Jensen AL, Johansson PI, Kjelgaard-Hansen M, Rozanski E, Tranholm M and Kristensen AT** (2010) Development of a model based scoring system for diagnosis of canine disseminated intravascular coagulation with independent assessment of sensitivity and specificity. *The Veterinary Journal* **185**, 292–298.
- Yii CY, Chen CY, Fresh JW, Chen T and Cross JH** (1968) Human angiostrongyliasis involving the lungs. *Chinese Journal of Microbiology* **1**, 148–150.